Fingering Instabilities in Variable Viscosity Miscible Fluids: Radial Source Flow

Vandita Sharma[*1], Satyajit Pramanik[1, 2] and Manoranjan Mishra[1]
[1]Department of Mathematics, Indian Institute of Technology Ropar, Rupnagar 140001, India
[2] Nordic Institute for Theoretical Physics (NORDITA), SE-10691 Stockholm, Sweden
*Correspondence author: Email address: vandita.sharma@iitrpr.ac.in

Abstract: Viscous fingering (VF), a hydrodynamic instability, is often observed in porous media while displacing fluids having viscosity mismatch. Here, for the first time, we present the COMSOL® simulations of the radial displacements of miscible fluids in a two dimensional (2D) homogeneous porous medium. It is shown that, even with an unfavourable viscosity contrast between the two fluids, it is possible to have a stable displacement, that is, the absence of the fingering instability. Also, the evolution from 'flowers' to 'branches' is discussed. The results of the present simulations are in accordance with the linear stability results.

Keywords: Hydrodynamic instability, Viscous fingering, Miscible fluids, Radial source flow, Pattern formation.

1. Introduction

From oil recovery [1,2] to chromatographic separation [3]; CO_2 sequestration [4] to aquifer contamination, VF is discerned in many areas and has attracted a large number of researchers over several decades. Both experimental and theoretical studies of VF have considered two kinds of displacement models, viz., radial [2,5-10] and the rectilinear [1,3,4,11]. Both these displacement processes are equally applicable for miscible as well as immiscible fluids but have some dissimilarities. The major difference in the rectilinear and the radial displacements lies in the growth of perturbations, which is exponential for the former [1] while algebraic for the latter [7]. Although both the displacement processes are associated with a critical Péclet number [7,11] for the onset of instability; this critical number depends on the frozen diffusive time t_0 only for the rectilinear model [11], while the radial model witnesses no such dependence. An asymmetric interface and multiple stages of instability are observed in radial flow [12]. The different dynamics for the rectilinear and the radial displacement model can be explored further.

The rectilinear displacement model is helpful in studying chromatographic separation [3], carbon dioxide sequestration [4], oil recovery, etc. In 1981, Paterson [2] pointed out that injection of fluid to extract oil is an example of radial displacement as the fluid is being injected through a well (a point source). In various chemical reactions, the reactant/autocatalyst is injected radially [5]. Another fascination of viscous fingering in radial displacement is the complex pattern formation, which greatly resembles with many physical and ecological processes observed in nature. Diffusion-limited aggregation [13], crystal growth [14], the growth of the bacterial colonies and snowflake formation [6], arrangements of leaves in different plants/trees, etc. are a few such processes from a long list. Thus, the study of pattern formation in radial displacements can greatly help to relate different aspects of nonlinear dynamics across various disciplines. This motivates the present paper.

Many theoretical [7,12], experimental [2,5,6,9] and numerical [6,8] studies of the radial displacements have been carried out in the past. To the best of the author's knowledge, this paper discusses COMSOL® simulations of the miscible displacement in radial source flow for the first time in literature. Different mesh available in COMSOL® are explored. The observed patterns are discussed and it is shown that the viscous fingering instability can be suppressed or increased by controlling various flow parameters.

2. Governing equations

The radial displacement is modeled by considering a circular domain with an injection hole (inlet) in the center. A viscous fluid is injected from this hole into the circular domain, which is saturated with another viscous fluid. The fluids considered are Newtonian, incompressible, miscible, neutrally buoyant and

non–reactive. The two fluids are two different solutions of a solute dissolved in a solvent. The initial concentration level of the solute in the two fluids is different, and mixing of the two fluids drives the concentration gradient between the two fluids towards an equilibrium state of uniform concentration in the mixture. The problem under discussion has two parts:

The hydrodynamic part which deals with the flow of the fluid and **the transport of species part** which describes the concentration of the species.

Mathematical modeling of the above mentioned physical problem is described in terms of coupled nonlinear partial differential equations [7], as follows:

Continuity equation:

$$\vec{\nabla}\cdot\vec{u} = 0 \qquad (1)$$

Darcy's law:

$$\vec{\nabla}p = -\frac{\mu(c)}{\kappa}\vec{u} \qquad (2)$$

Convection-Diffusion equation :

$$\varepsilon\frac{\partial c}{\partial t} + \vec{u}\cdot\vec{\nabla}c = \vec{\nabla}\cdot(D\vec{\nabla}c) \qquad (3)$$

In these equations, $\vec{u}$ is the Darcy velocity; κ and ε are respectively the permeability and porosity of the medium; c is concentration of the species; D is the molecular diffusion coefficient; μ is the dynamic viscosity of the fluid, which depends on the concentration of the fluid. We assume the relation to be monotonic which can be written as

$$\mu(c) = \mu_1 \exp(Rc) \qquad (4)$$

where $R = \ln(\mu_2/\mu_1)$ is the log-mobility ratio, μ_1 and μ_2 are the dynamic viscosity of the displacing and the displaced fluid, respectively**.** Equations (1) and (2) deal with the hydrodynamic part, representing the conservation of mass and the conservation of momentum, respectively. Equation (3) is the convection-diffusion equation, which describes the transport of species.

The initial and the boundary conditions for the hydrodynamic part comprise of specifying the velocity and/or the pressure. Initially, there is no flow. Uniform velocity is maintained at the inlet, while there is free flow at the outlet. Mathematically, this can be written as follows:

$\vec{u}\,(x,y) = 0$ at $t = 0$ for all x and y.

$$\hat{n}\cdot\vec{u} = \begin{cases} 0, & \text{at the outlet} \\ U_0, & \text{at the inlet}, \end{cases} \qquad \text{for } t > 0.$$

Similarly, we have one fluid of concentration c_1 initially in the domain. A fluid of concentration c_2 is injected continuously and no flux in concentration is needed at the outlet. Mathematically, these initial and boundary conditions for the transport of species part can be specified as:

$$\left.\begin{array}{l} c(x, y) = c_2, \text{ at the inlet} \\ (\hat{n}\cdot\vec{\nabla})c = 0 \text{ at the outlet.} \end{array}\right\} \quad \text{for } t > 0$$

$c(x, y) = c_1$, inside the domain at $t = 0$, for all x and y. Here $\hat{n}$ is the outward unit normal.

3. Use of COMSOL Multiphysics® Software

Two-Phase Darcy's Law (tpdl) model of the Fluid Flow module is used for the simulations. It solves Darcy's law for the total pressure and the transport of the fluid content for one fluid phase. The domain of simulations and the physical properties of the fluids are shown in figure 1. Various parameters used are given in table of data in appendix. The equations used in this model are:

$$\frac{\partial\varepsilon_p\rho}{\partial t} + \vec{\nabla}\cdot\rho\vec{u} = 0 \qquad (5)$$

$$\vec{u} = -\frac{\kappa}{\mu}\vec{\nabla}p \qquad (6)$$

$$\rho = s_1\rho_1 + s_2\rho_2 \qquad (7)$$

$$\frac{1}{\mu} = s_1\frac{\kappa_{r1}}{\mu_1} + s_2\frac{\kappa_{r2}}{\mu_2} \qquad (8)$$

$$s_1 + s_2 = 1 \qquad (9)$$

$$\frac{\partial\varepsilon_p c_1}{\partial t} + \vec{\nabla}\cdot(c_1\vec{u}) = \vec{\nabla}\cdot(D_c\vec{\nabla}c_1) \qquad (10)$$

where $c_1 = s_1\rho_1$. In the above equations, ε_p and κ are respectively the porosity and the permeability of the porous medium; D_c is the capillary diffusion; ρ is the density of the fluid. For $j = 1, 2$, s_j is the fraction of void space occupied by the fluid j, called as saturation of fluid j. ρ_j, μ_j and c_j are the density, viscosity and

concentration of fluid j. κ_{rj} is the relative permeability of fluid j, that is, the conductance offered by porous medium to a fluid relative to other fluid.

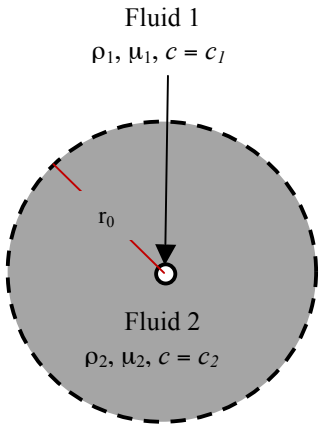

Figure1: Schematic of the radial displacement.

Now, we will explain the equivalence of the equations (5) - (10) to equations (1) - (3). We have assumed the fluids to be neutrally buoyant so we have $\rho_1 = \rho_2 = \rho$, hence equation (7) and (9) are identical. Equation (9) follows from the definition of saturation given in previous paragraph. In the tpdl, capillary model of porous medium is considered. In this model, the porous medium is assumed to be one consisting of pores which are modeled as capillary tubes, the fluid flows through these tubes and we have conservation of mass and momentum as given by equations (5) and (6) using the continuum approach. Without loss of generality, we take the values of s_1 to be zero or one, which represent the fluid to be only fluid 1 or fluid 2. The value of s_j between zero and one represents the mixing zone or the interface, where the two fluids have mixed together and co-exist. It should be noted that the schematic in figure 1, in no way represents a capillary tube, it is the macroscopic view of the porous medium consisting of the pore space and the solid matrix. The material properties are incorporated in terms of the porosity and the permeability.

Equation (5) represents conservation of mass and reduces to equation (1) as we have constant porosity and incompressible fluids. Equations (6) and (2) are the same and represent the Darcy's law with $\vec{u}$ being Darcy velocity. Equation (10) is convection-diffusion equation, which reduces to equation (3) using constant porosity of the medium, incompressibility of the fluid and $D_c = \varepsilon_p D$. Equation (8) is the viscosity-concentration relationship, which can be shown to be similar to equation (4) as follows:

For $j = 1, 2$, we assume $\kappa_{rj} = 1$ and the viscosity of fluid j, as

$$\mu_j = \mu_1 \exp(R \cdot s_1) \qquad \textbf{(11)}$$

Hence from equation (8) we get,

$$\frac{1}{\mu} = \frac{1}{\mu_1 \exp(R \cdot s_1)}(s_1 + s_2)$$

Now using equation (9), we get the viscosity concentration relation consistent with equation (4).

Next we explain the boundary and initial conditions. The 'inlet' and the 'outlet' boundary conditions of the tpdl model are consistent with the boundary conditions specified in the previous section and they are prescribed respectively at the inlet (inner circle) and the outlet (dashed boundary) [see figure1]. Initial condition is given by specifying value of s_1 and pressure $p = 0$, which guarantees no flow initially as at the outlet also, $p = 0$.

Extra fine 'Free Triangular' mesh of Fluid dynamics is used in the simulations. Also a customised quadrilateral mesh (Free Quad), gave the patterns similar to the one obtained using triangular mesh. But in case of mapped mesh, a disturbance has to be given at a suitable distance from the injection hole for instability to occur. See appendix for more details.

4. Results and discussions

First of all, we discuss the evolution from 'flowers' to 'branches'. Keeping the flow rate Q, and the diffusion coefficient D fixed, a variety of patterns are observed on increasing the log-mobility ratio $R(>0)$. For smaller R, wide fingers are observed, whose tips at different times appear to be lying on concentric circles [10]. Beautiful flower-like patterns are formed for smaller R. As we go on increasing R, the fingers get narrower, tip splitting occurs, resulting in ramified structures. Hence on increasing R, an evolution from flowers to branches is observed as is evident from figure 2. In all the figures,

blue fluid is less viscous while the red fluid is more viscous one.

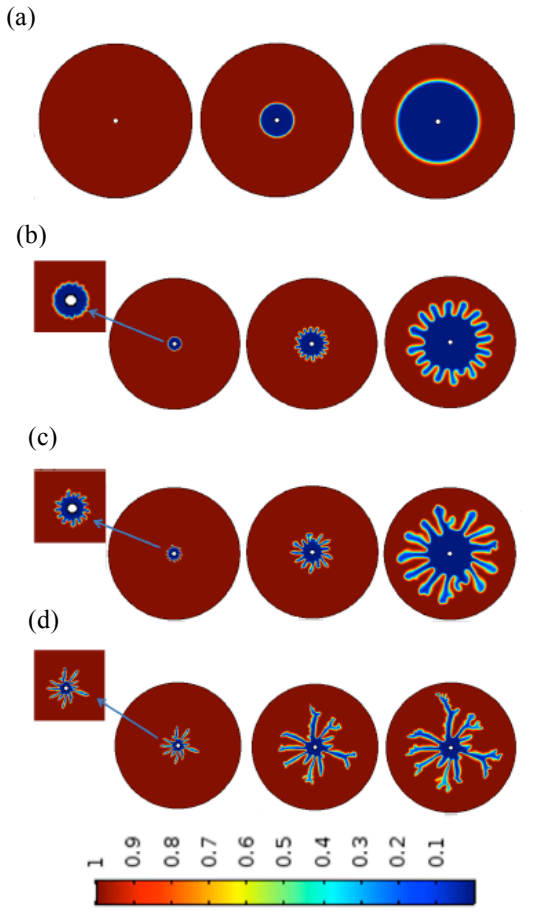

Figure 2: From 'flowers' to 'branches': Spatio-temporal evolution of fluid saturation s_1 for U_0 = 2 mm/s, D = 10^{-8} m^2/s and (a) R = 0 at t = 0, 10, 60 seconds; (b) R = 2 at t = 2, 10, 60 seconds, (c) R = 3 at t = 2, 10, 60 seconds, (d) R = 5 at t = 5, 20, 30 seconds. Clearly in (b), we have flower-like patterns which turn into branches on increasing R, as we move to (d).

Also, from the zoomed out part, it is evident that on increasing R, the fingering instability is observed early, as we see more prominent fingers in figure 2(c) than in figure 2(b) at time t = 2 seconds. Hence, we can say that more the viscosity contrast between the fluids, more unstable is the interface. Next, we discuss how the viscous fingering instability can be suppressed/reduced by changing different flow parameters. In our simulations we capture that for a fixed R and D, the number of fingers, their morphology can be controlled by changing the flow rate Q. It is evident that for the same R and D as in figure 2, fingering instability reduces significantly by reducing the flow rate Q [see figure 3].

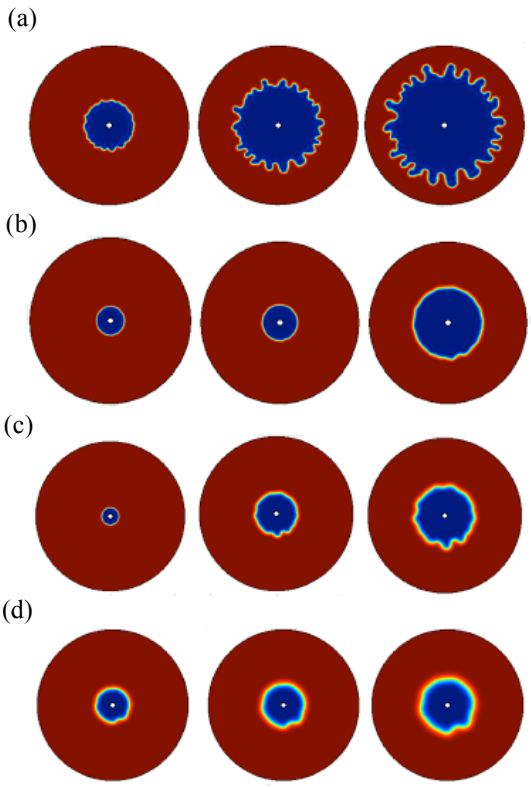

Figure 3: Decrease in the viscous fingering instability: Spatio-temporal evolution of fluid saturation s_1 for D = 10^{-8} m^2/s and (a) R = 1, U_0 = 20 mm/s at t = 2, 6, 10 seconds; (b) R = 1, U_0 = 2 mm/s at t = 2, 10, 60 seconds, (c) R = 2, U_0 = 0.5 mm/s at t = 10, 60, 120 seconds, (d) R = 3, U_0 = *0.2* mm/s at t =100, 160, 250 seconds. From (a) & (b), it is evident how decreasing Q, keeping R, D fixed, suppresses fingering instability. Same is clear if we compare 3(c, d) with 2(b, c), respectively.

This result is in accordance with the linear stability analysis (LSA) results of Tan & Homsy

[7]. We know from LSA, that the most dangerous wavenumber is directly proportional to Q, so decreasing flow rate results in decreased maximum wavenumber, hence the most unstable wavelength increases. Thus, less or no fingers are observed on decreasing Q.

By keeping Q and R fixed but varying D, we could obtain a stable displacement even for unstable viscosity contrast between the fluids. From figure 4, we notice that whatever R and Q

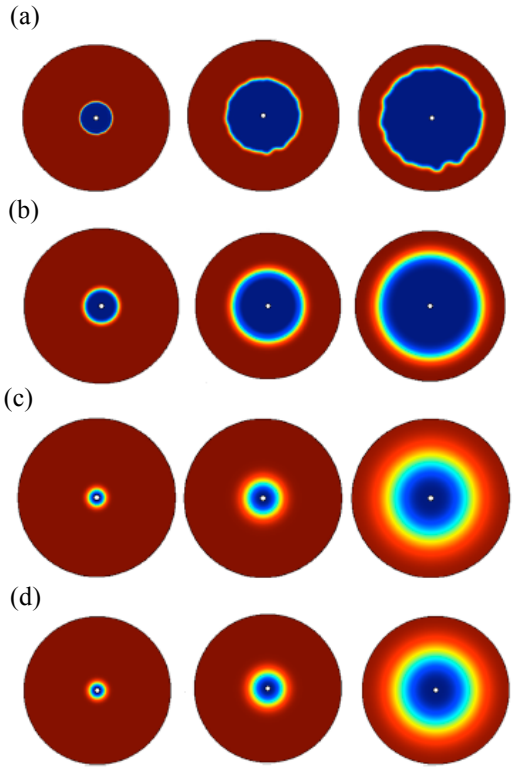

Figure 4: Decrease in the viscous fingering instability: Spatio-temporal evolution of fluid saturation s_1 for (a) $D = 10^{-7}$ m^2/s $R = 1$, $U_0 = 20$ mm/s at $t = 1, 5, 10$ seconds; (b) $D = 10^{-6}$ m^2/s, R=1, $U_0 = 20$ mm/s at t = 1, 5, 10 seconds, (c) D =10^{-6} m^2/s, R = 2, U_0 = 2 mm/s at t = 2, 10, 60 seconds, (d) D =10^{-6} m^2/s, R = 3, U_0 = 2 mm/s at t =2, 10, 60 seconds. From (a), (b) & 3(a), it is evident how increasing D, keeping R, Q fixed, suppresses fingering instability. Same is observed if we compare 4(c, d) with 2(b, c) and 3(c, d), respectively.

be, for $D \leq 10^{-6}$ m^2/s, the fingering instability is suppressed and the interface undergoes a stable displacement similar to the one in $R = 0$ case, see figure 2(a). This is in accordance with the LSA results of Tan and Homsy [7], that there exists a critical Péclet number for the onset of instability. Since Péclet number is inversely proportional to diffusion coefficient, on increasing D, the Péclet number decreases and we don't observe any fingering instability at the interface. This can also be explained in terms of diffusion-advection dominance. For larger D, the diffusive time is always less than the advective time [9] and hence, diffusion dominates advection so that the fingers are not observed.

5. Conclusions

Using COMSOL Multiphysics®, we successfully simulate the suppression, decrease or increase of miscible VF in radial displacement in a 2D homogeneous porous medium by varying the parameters R, Q and D. For a fixed D and Q, it is observed that the fingering instability occurs earlier and the fingers get steeper as R increases. A transition from 'flowers' to 'branches' is observed with increasing R. On the other hand, on increasing D, keeping Q and R fixed, the interface was observed to approach the stable displacement. This confirms the existence of a critical Péclet number for the onset of fingers. For a given Q and R, increasing D, beyond the limit of the critical value of the Péclet number, results into a stable displacement of the front. The same can be observed while decreasing Q and keeping R and D unchanged. Our simulation results are in accordance with the linear stability results of Tan & Homsy [7] and the theoretical results of Chui *et al.* [9]. We also observed that the tips of forward and backward fingers lie on concentric circles as pointed out by Bischofberger *et al*. [10]. Also, we explored how to get qualitatively and quantitatively similar patterns using different meshing. Understanding the pattern formation, fractal dimension, and many other interesting features of radial displacement of the miscible fluids in homogeneous as well as heterogeneous porous media are the focuses of our ongoing research.

6. References

[1] G.M. Homsy, Viscous fingering in porous media, *Annu. Rev. Fluid Mech.*, **19**, 271-311 (1987).

[2] L. Paterson, Radial fingering in a Hele Shaw cell, *J. Fluid Mech.,* **113**, 513-529 (1981).

[3] M. Mishra, M. Martin and A. De Wit, Differences in miscible viscous fingering of finite width slices of positive or negative log-mobility ratios, *Phys. Rev. E,* **78**, 066306 (2008).

[4] H.E. Huppert and J.A. Neufeld, The fluid mechanics of carbon dioxide sequestration, *Annu. Rev. Fluid Mech.,* **46**, 255-272 (2014).

[5] Y. Nagatsu, K. Matsuda, Y. Kato and Y. Tada, Experimental study on miscible viscous fingering involving viscosity changes induced by variations in chemical species concentrations due to chemical reactions, *J. Fluid Mech.,* **571**, 475-493 (2007).

[6] S. Li, J.S. Lowengrub, J. Fontana and P. Palffy-Muhoray, Control of viscous fingering patterns in radial Hele-Shaw cell, *Phys. Rev. Lett.,* **102**, 174501 (2009).

[7] C.T. Tan and G.M. Homsy, Stability of miscible displacements in porous media: Radial source flow, *Phys. Fluids,* **30 (5)**, 1239-1245 (1987).

[8] S. Li, J.S. Lowengrub and P.H. Leo, A rescaling scheme with application to the long-time simulation of viscous fingering in a Hele-Shaw cell, *J. Comput. Phys.,* **255(1)**, 554-567 (2007).

[9] J. Y. Y Chui, P. de Anna and R. Juanes, Interface evolution during radial miscible viscous fingering, *Phys. Rev. E,* **92**, 041003(R) (2015).

[10] I. Bischofberger, R. Ramachandran and S.R. Nagel, Fingering versus stability in the limit of zero interfacial tension, *Nat. Commun.*, **5**, 5265 (2014) .

[11] S. Pramanik and M. Mishra, Effect of Péclet number on miscible rectilinear displacement in a Hele-Shaw cell, *Phys. Rev E,* **91**, 033006 (2015).

[12] J.A. Miranda and M. Widom, Radial fingering in a Hele-Shaw cell: a weakly nonlinear analysis, *Physica D*, **120**, 315-328 (1998).

[13] T.A. Witten Jr. and L.M. Sander, Diffusion-limited aggregation, a kinetic critical phenomenon, *Phys. Rev. Lett.,* **47**, 1400 (1981).

[14] J.S. Langer, Instabilities and pattern formation in crystal growth, *Rev. Mod. Phys.,* **52**, 1 (1980).

7. Appendix

A) TABLE OF DATA

Symbols	**Parameters**	**Value and units**
R	Log mobility ratio	0, 1, 2, 3, 5
U_0	Injection velocity	0.002 m/s, 0.02 m/s & 0.05m/s
μ_1	Viscosity of the displacing fluid	1 mPa*s
r_i	Radius of the inlet	0.002 m
r_0	Radius of the outer circle	0.058 m
ε_p	Porosity of the medium	0.5
κ	Permeability of the medium	10^{-9} m^2
D	Molecular diffusion coefficient	$10^{-6} - 10^{-10}$ m^2/s

B) MESHING:

We verify the dependence on the mesh type of the observed fingering dynamics. For this purpose, we used three different types of mesh: (a) free triangular, (b) mapped, and (c) quadrilateral. The free triangular mesh is discussed in the main text of this paper. Here, we present a brief discussion of the other two mesh types. Mapped mesh used for the domain discretisation in simulations is constructed using Bézier polygon. Distribution properties under mapped mesh are adjusted to get the desired mesh. Figure below shows a typical mapped mesh.

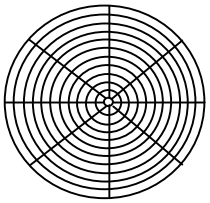

Figure: Mapped mesh.

Initial condition used to ensure the fingering instability is :

$$c(x,y) = \begin{cases} 1, & x^2+y^2 < r_0^2 \\ 0.01 * rn(x,y), & x^2+y^2 < r^2 \end{cases}$$

where 'r' is to be chosen appropriately for the instability to trigger; $rn(x, y):R^2 \rightarrow [0, 1]$ is a normally distributed random function with mean 0.5 and variance 1. Inlet and outlet conditions remain the same as mentioned in the section 3. The fingering patterns obtained using mapped mesh are qualitatively the same as those obtained using free triangular mesh.

The quadrilateral mesh (Free Quad) is customized and used for the simulations. The patterns obtained are quantitatively and qualitatively similar to those obtained using the triangular mesh [shown in figure below].

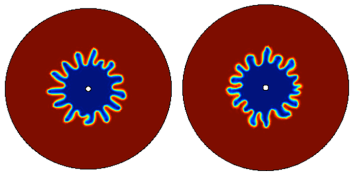

Figure: Spatio-temporal evolution of fluid saturation s_1 at t = 30 seconds, R = 2, U_0 = 2 mm/s, D = 10^{-8} m^2/s corresponding to free triangular mesh (left) and free quadrilateral mesh (right).

C) DIFFERENT SOLVERS:

For the simulations in this paper, we have used direct solvers as they are more robust than iterative solvers. Different direct solvers, such as MUMPS, PARDISO and SPOOLES are used for the optimal computation (CPU) time and numerical accuracy. It is observed that the direct solver SPOOLES is the slowest among the three solvers, while the time taken by MUMPS and PARDISO are comparable. Among the latter two solvers, PARDISO is relatively faster compared to MUMPS. The number of the degrees of freedom for all the solvers were 42138.

Parameter / Solver	R = 2	R = 3
MUMPS	204 sec	378 sec
PARDISO	157 sec	267 sec
SPOOLES	354 sec	-

Table: Comparison of computation (CPU) time for different direct solvers. Parameters used in all these simulations are U_0 = 2 mm/s and D = 10^{-8} m^2/s. Extra fine fluid dynamics triangular mesh is used in these simulations.